NIKHEF PROJECT PLAN: CRYOLINKS
Cryogenic vacuum links to isolate interferometer arms for Advanced Virgo

Suspension system

J.F.J. van den Brand[1],
[1] *Nikhef, National Institute for Subatomic Physics*,
P.O. Box 41882, Amsterdam, the Netherlands

May 10, 2011

email address: jo@nikhef.nl

Procedure start date	01/10/2009
Procedure end date	01/10/2013
Document version	v01r01
Version date	05/05/2011

Abstract

The current Virgo vacuum level needs to be improved by about a factor of hundred in order to be compliant with the required Advanced Virgo sensitivity. Such an improvement requires baking out the interferometer arms. To separate these arms from the towers that hold the mirrors and allow the bake-out, four cryogenic vacuum links will be installed. It is important that the beam pipes are isolated against possible bubble noise from the cryolinks. This note discussions the suspension system.

Contents

1 Introduction

Heat is dissipated in the liquid nitrogen (LN2) bath of the cryolinks and gas bubbles will be formed. It is important that possible displacement noise induced by bubbling is attenuated for Advanced Virgo. Therefore, the inner aluminum vessel that holds the LN2 will be suspended from the stainless steel UHV vessel by using two double air springs, in combination with longitudinal and transverse suspension systems. The mechanical design is shown in Fig. 1.

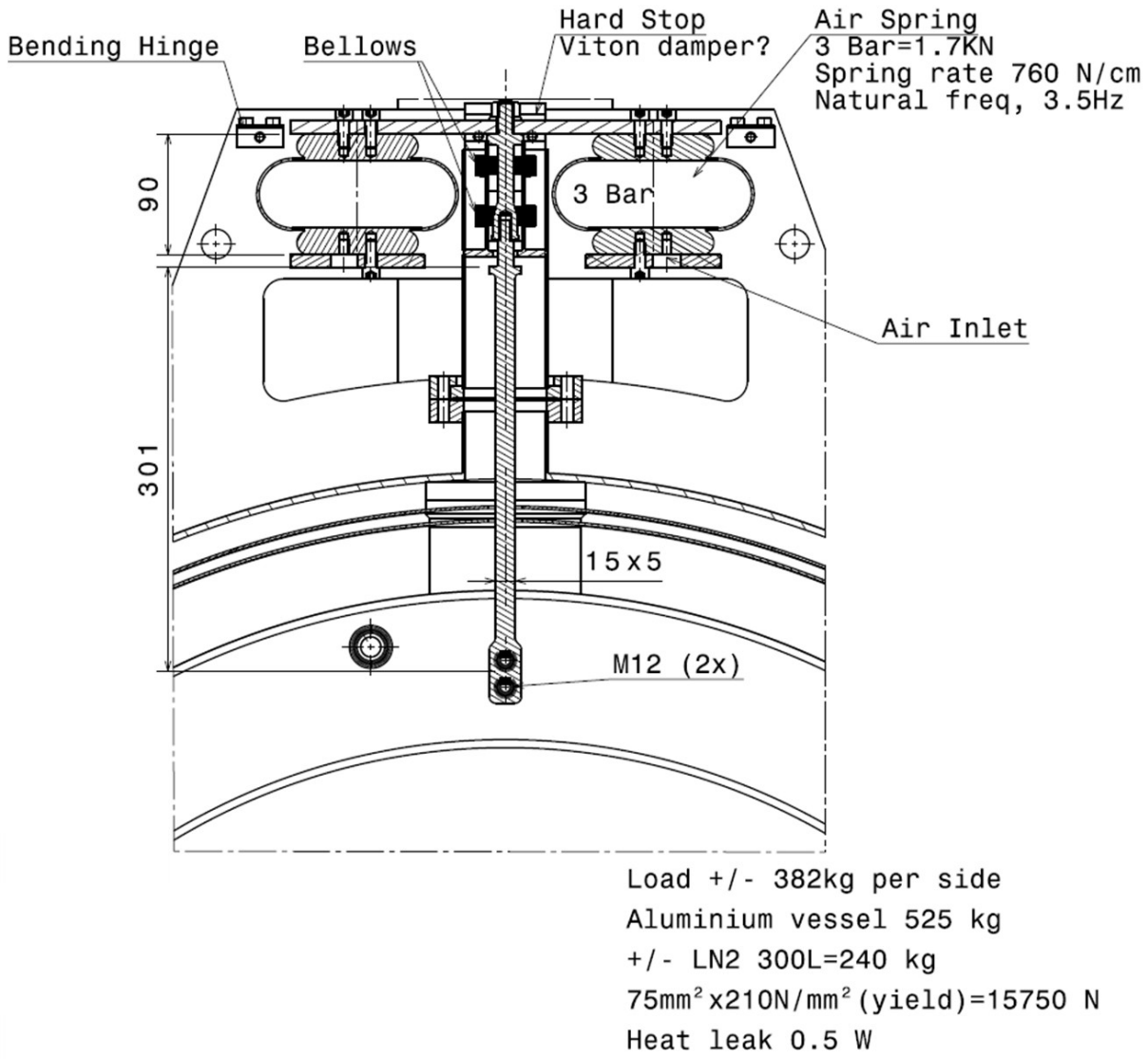

Figure 1: *The cold vessel of the cryolink is suspended with air springs in order to isolate Advanced Virgo from possible bubbling noise in the LN2.*

Care is taken to minimize the development of gas buffles. A phase separator is placed between the LN2 storage system and the cryolink to remove the gaseous nitrogen (GN2). The LN2 inlet has been designed such that LN2 will flow smoothly into the bath (laminar flow is ensured by the design), in this manner minimizing any induced noise from bubbling. The liquid nitrogen level in the bath can be controlled to within ± 10 mm, by admitting the LN2 through a PID

controlled needle valve. The valve is mounted such as to minimize heat input from the transfer line and the heat leak through its needle shaft, in this way minimizing gas formation. Note that the bath has a sizable width of about 550 mm. Again this guarantees that bubbles have a large escape path to the surface over the entire 2000 mm length of the cryotrap.

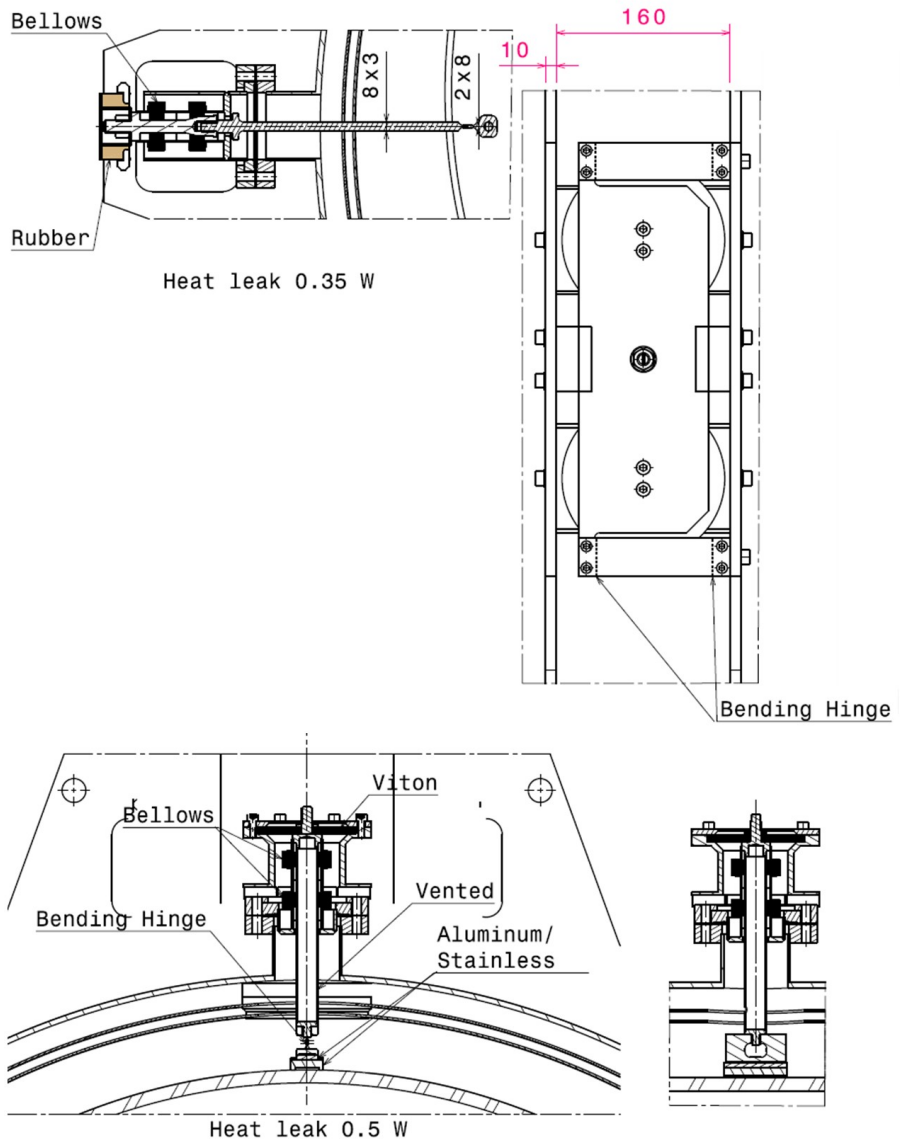

Figure 2: *Suspension system for the cryolink. Left: silicon rubber spring for horizontal positioning; middle: air-spring system for vertical isolation; right: top view of the flexible hinges. See Fig. 1 for a cross section of the central air spring suspension system.*

The cryolink and baffle system will experience displacement noise from seismic motion of the floor and possibly bubble induced noise. We intend to incorporate a well-damped suspension system based on air-springs to isolate the system from bubble noise produced by the cold LN2 part. The LN2 vessel is connected to the vacuum vessel via this system. The resonance frequency is about 3 - 4 Hz and the Q-factor about 10 to 20. A well-damped system is needed since there will always be up-conversion from low frequencies (around 0.5 Hz) or modes at low frequencies. High-frequency noise from bubbles may influence the sensitivity of Advanced Virgo through

back-scattering.

The various elements of the suspension system are shown in Fig. 2. The silicon rubber spring for horizontal positioning allows movement from thermal contraction/expansion and specifically retricts motion in the xy-plane (transverse). The air-spring system for vertical isolation needs to allow vertical motion *e.g.* during bake-out. The flexible hinges located at the top provide guidance for vertical displacement (but not horizontal) of the top of the air springs. It has to be investigated to what extend the bellows by-pass the suspension isolation. Note that in case it is judged favorably to discard of the suspension system, that it can be replaced by fixed mounts, without affected the rest of the cryolink.

2 Experience at Virgo

A preliminary simulation of noise from back-scattered light from the cryolinks of Advanced Virgo has been carried out by Fiori [1]. It is based on the noise model described in Ref. [2] and realistic seismic noise (see Fig. 3) obtained from the measured horizontal displacement of the existing Virgo cryogenic trap. Fig. 3 shows the following characteristic noise features

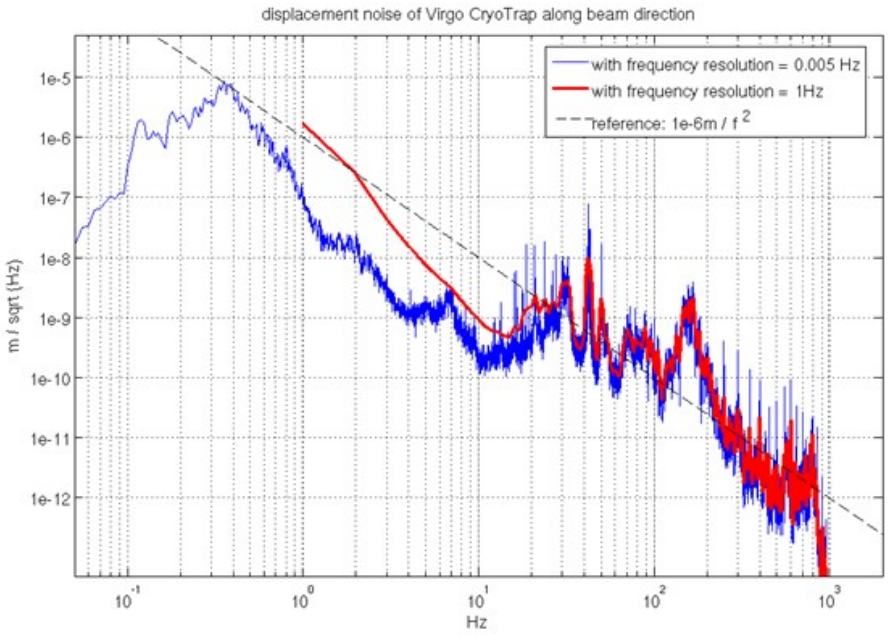

Figure 3: *Vibration noise along the beam axis of the existing Virgo cryotrap. The spectrum is measured with a frequency resolution of 1 Hz (the red curve shows the rms value) and with a frequency resolution of 0.005 Hz (blue curve) which is resolving all pseudo-monochromatic vibrations produced by mechanical rotating devices (e.g. fans, engines) located in the CB hall. The dashed line shows the reference noise spectrum of* $10^{-6}/f^2$ *m/*$\sqrt{\text{Hz}}$. *From Ref. [1].*

- A large bump at 0.4 Hz which is associated with sea activity, and in worst conditions (a few % of the time) can reach amplitudes of about 10 μm.

- Several narrow peaks above 10 Hz, which originate from rotating devices in the experimental hall (*e.g.* cooling fans, engines). These peaks have a quality factor Q which is measured to never exceed a value of 2000. The narrowest peaks (in the range from 10 to 50 Hz) have a measured width of 0.01 Hz.
- The noise around 50 - 150 Hz is enhanced (see Virgo's eLogs 24753 and 23722) by about 5 times by the action of LN2 bubbles after LN2 refill operations. The excited peaks probably correspond with mechanical resonances of the existing Virgo cryolink. Such resonances should be avoided in the AdV cryolinks.

3 Upconversion noise model

The scattered light can be estimated by considering an optical path where photons undergo a first scattering event at the mirror surface towards any exposed cryolink walls, then a second pure back-scattering event from the cryolink walls back to the mirror, and a final scattering by the mirror into the ITF beam solid angle. The resulting scattered light noise is given by (see Ref. [2])

$$h_{\rm sln}(t) = \kappa \sin\left(\phi(t) + \Phi_0\right), \tag{1}$$

with $\phi(t) = \frac{4\pi}{\lambda} z(t)$ the phase delay of the scattered field with respect to the main beam, $z(t)$ the displacement of the cryolink walls along the beam direction. The angle Φ_0 is the static phase difference between the scattered field and the main field. The coupling factor κ depends on geometrical parameters and scattering properties of the mirror and trap walls. It has been estimated at $\kappa = 2 \times 10^{-25}$ m/$\sqrt{\rm Hz}$ [3]. When the displacement noise of the cryolinks is small,

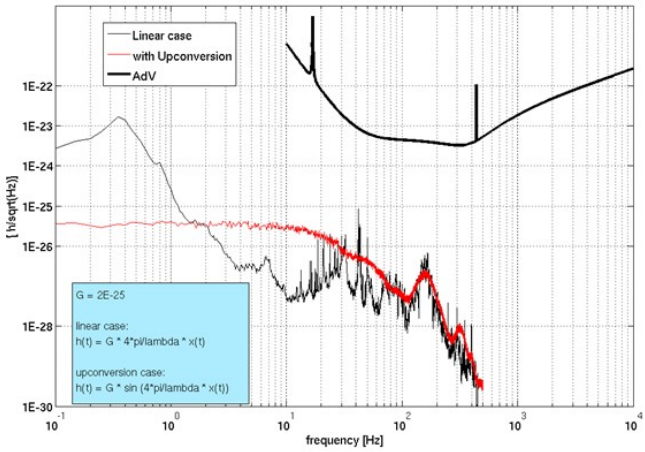

Figure 4: *Projected noise from AdV cryotrap for* $\kappa = 2 \times 10^{-25}$ *m/*$\sqrt{\rm Hz}$ *and assuming that the vibration noise is the same as that of the existing Virgo cryotrap. The predicted noise (red curve) is compared to the prediction from the linear approximation (black curve), and to the AdV design sensitivity. From Ref. [1].*

$z(t) \ll \frac{\lambda}{4\pi} \approx 10^{-7}$ m, then Eq. (1) can be approximated by

$$h_{\rm sln}(t) = \kappa \frac{1}{\sqrt{2}} \frac{4\pi}{\lambda} z(t), \tag{2}$$

and Fig. 3 shows that the linear case condition ($z(t) < 10^{-8}$ m) holds for most of of the vibration noise spectrum (exceptions are the microseism and the cooling fans that around 50 Hz). Note that in the linear case the scattered field vector undergoes small angular displacements around its position (Φ_0) and the averaging of the slow drift of the static phase leads to the term $1/\sqrt{2}$. The results for the linear case are shown in Fig. 4.

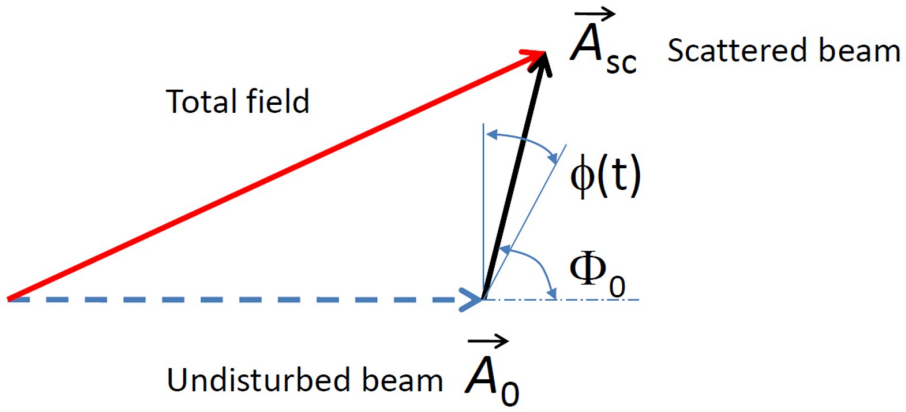

Figure 5: *Schematic representation of the scattered field A_{sc}, its phase Φ_0 with respect to the ITF beam A_0, and its changing phase angle $\phi(t)$. From Ref. [1].*

For large vibration noise ($z(t) > 10^{-8}$ m) the non-linear term in Eq. (1) cannot be neglected. The behavior of spectral noise in the non-linear case has been described in Refs. [**?**, **?**, **?**] and can be understood as follows. Each time $z(t)$ changes by $\lambda/2$ the phase angle $\phi(t)$ varies by 2π. Thus the scattered field vector (see Fig. 5) completes one full turn and $h_{sln}(t)$ completes one oscillation. The number of such oscillations per second, *i.e.* the frequency of the strain noise, is

$$f_{\rm sln} = \frac{2}{\lambda}\dot{z}(t), \tag{3}$$

where, $\dot{z}(t)$ is the velocity of the walls of the cryolink, the first order time-derivative of $z(t)$. In the special case (which is often valid) that the wall-vibration of the cryolink is monochromatic, $z(t) = A_0 \sin(2\pi f_0 t)$, Eq. (3) gives the maximum frequency of the h_{sln} spectral noise as

$$f_{\rm max} = \frac{4\pi}{\lambda} A_0 f_0. \tag{4}$$

Qualitatively, what happens is that a monochromatic displacement noise (A_0, f_0) produces a shoulder in the $h_{\rm sln}$ spectrum which extends up to $f_{\rm max} > f_0$ (so-called 'up-conversion'), and has an rms value $\sigma(h_{\rm sln}) = \kappa\sqrt{\frac{2}{f_{\rm max}}}$ (see Ref. [4]).

Fig. 4 compares the predicted noise of backscattering, using both the non-linear (red curve) and linear (black curve) approximation for intense micro-seismic activity. The effect of up-conversion of the micro-seismic peak ($A_0 = 8 \times 10^{-6}$ m) is evident: the shoulder extends up to $f_{\rm max} \approx 35$ Hz, and has amplitude $\sigma(h_{\rm sln}) \approx 4 \times 10^{-26}$ m/$\sqrt{\rm Hz}$ as predicted by the above equations.

Fiori [1] deduces two simple rules for up-conversion noise in the detection band ($f_{\rm max} > 10$ Hz):

1. as long as κ guarantees a safe limit for the linear approximation, the up-conversion noise in the AdV detection bandwidth is limited as well. Its spectral amplitude is $\sigma((h_{\rm sln}) = \kappa\sqrt{\frac{2}{f_{\rm max}}} < \kappa$ (if $f_{\rm max} > 10$);

2. it seems a good safety rule to avoid the onset of up-conversion noise inside the ITF detection band ($f_{\max} > 10$ Hz) by

   (a) avoiding wall vibrations of the cryolink with frequencies $f > 10$ Hz and amplitudes $z > 10^{-8}$ m;

   (b) avoiding walls vibrations with frequencies $f < 10$ Hz and amplitudes z, such that $f \times z > \frac{\lambda}{4\pi} \times 10$, or velocities $v > \frac{\lambda}{2} \times 10$, *i.e* velocities greater than 5×10^{-6} m/s. This means that a possible resonance mode of the seismic isolation system of the cryolink, which for example is at $f = 5$ Hz should have amplitude $z < 10^{-7}$ m.

4 Air spring system

We propose to employ air suspensions from ContiTech AG. The lateral stiffness of air isolators differs greatly from type to type. In the cryolink construction part of the axial stifness is taken by the hinges. For the individual air isolator types, the following lateral stiffness values - relative to the axial stiffness - can be expected. The specified percentages are for the recommended operating height for vibration isolation.

- Single convolution air isolators 30 to 60%;
- double convolution air isolators 5 to 30%;
- belted air isolator 30 to 50%.

Triple convolution air isolators, rolling lobe air isolators and sleeve type air isolators have no positive lateral stiffness and can only be used for vibration isolation with lateral guidance. Lateral guidance can also be achieved on rolling lobe air isolators and sleeve type air isolators with the use of a restraining cylinder which turns the air isolator into a kind of guided diaphragm. Because of their low natural frequency, both types are excellent vibration isolators. However, we prefer to refrain from lateral guidance systems and propose to use single convolution isolators.

We have selected air-spring based isolators which are mounting elements of natural frequencies in the range 3.2 - 3.5 Hz. The spring force is obtained from the compression of the gases they contain. These isolators effectively suppress the transmission of vibration and structure-borne sound to the surroundings. Air isolators also reduce the effects of vibration by isolating sensitive equipment from the source. Damping limits vibration amplitudes to a permissible ratio. Lehr's damping ratio[1] D of standard air springs is 0.03.

The air isolators will be mounted so that the shortest distance between points of support is at least twice the height of the centre of gravity above the plane of support. This minimizes wobble and prevents operational problems. The spring stiffness of an air isolator results from the

[1] The damping factor θ (frequently given as a percentage and previously referred to as Lehr damping factor $D = \theta$) is a measure of the decrease in amplitude of a free decay process. Alternative and equivalent characteristics to describe the damping of a system are

- the loss factor $\eta \approx 0.5\theta$, and
- angular loss ξ (the phase angle between force and deformation, to be determined for $\eta = \tan \xi$).

It generally applies: the larger θ, the smaller are the maximum increase $z_{\max}(t)$ and the isolation effect of the excitation frequencies larger than 1.4 times the resonance frequency.

compression of the air volume it contains. The axial stiffness can be reduced further by using an auxiliary volume. This will be studied on the prototype. Depending on the dimensioning of the connection line between air isolator and auxiliary volume, a non-wearing, non-ageing air suspension system is created. If the connection line has a shut off system, the air spring suspension system can be switched between two vertical natural frequencies.

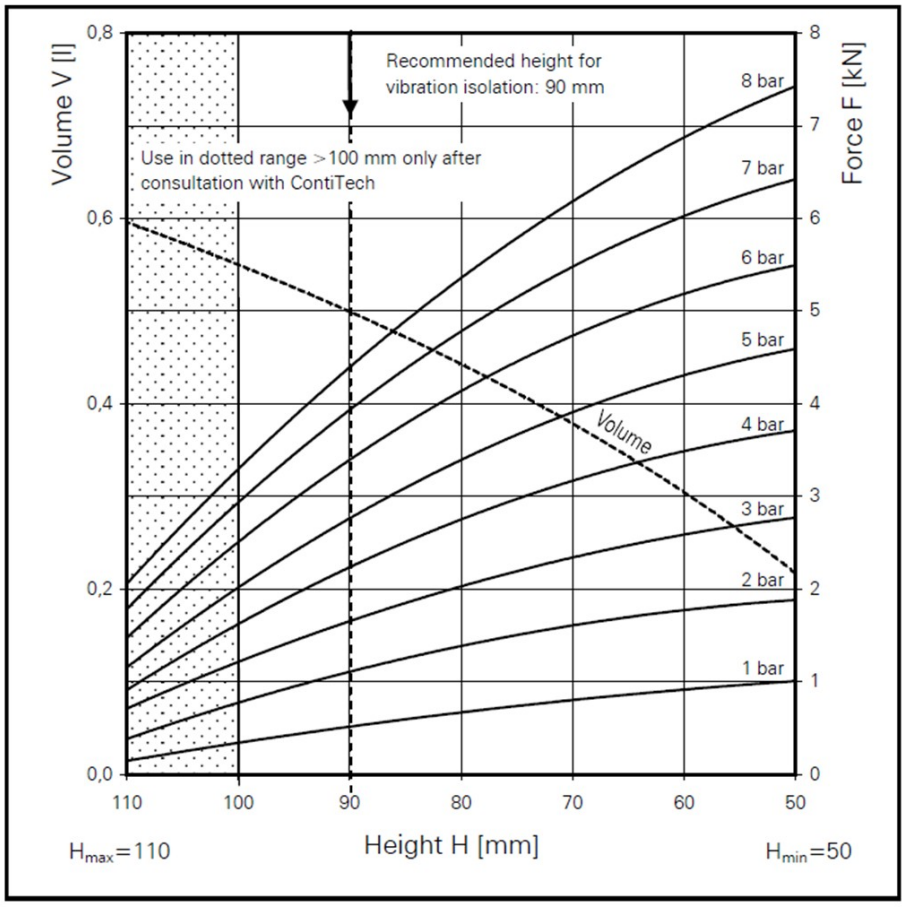

Figure 6: *Force height diagram for the FS 40-6 ContiTech single convolution air spring.*

We intend to employ the ContiTech FS 40-6 air spring. The aluminum vessel has a weight of 525 kg and will be filled with about 240 kg of LN2. This yields a 191 kg load per air spring. The force-height diagram is given in Fig. 6. Each spring needs an 160 mm diameter installation space. The recommended height of the spring is 90 mm (minimum is 70 mm). This height can be achieved with different combinations of applied pneumatic pressure and force load. The pressure should range from 3 to 8 bar (the corresponding force load then ranges from 1.7 to 4.4 kN). Spring rates range from 760 to 1820 N/cm and the natural frequency decreases from 3.5 Hz at 3 bar to 3.2 Hz at 8 bar.

5 Test results

We realized a test setup at Nikhef to determine the effectiveness of the suspension system and to measure the transfer function of the cryogenic shield suspension. The setup consists of a realistic

cross section of the cryolink, but with limited length. In order to mimic the LN2 load, the inner vessel is filled with water. The inner vessel is suspended from the outer stainless steel vessel through air springs. In addition, the system that constrains sideways motion is included. The set-up is shown in Fig 7.

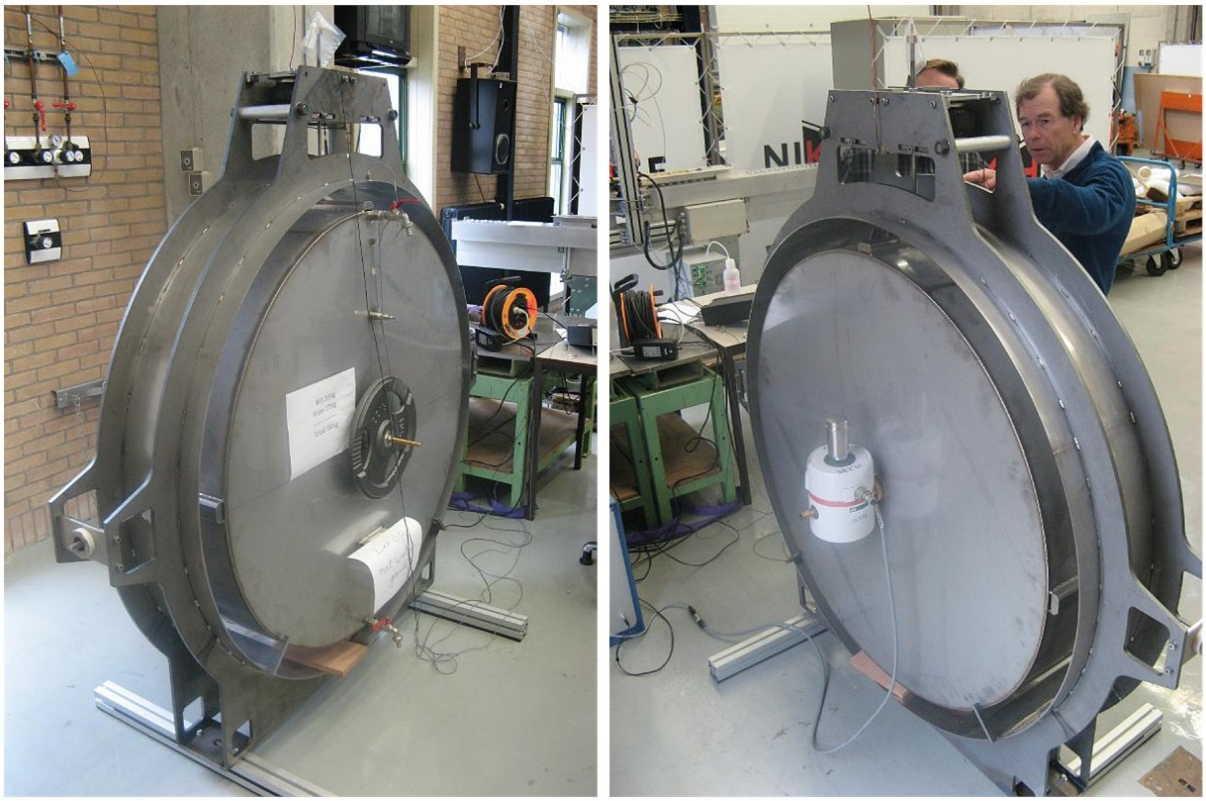

Figure 7: *Photographs of the test stand for measuring the attenuation performance of the suspension system envisioned for the cryolinks of Advanced Virgo.*

The measurements have been performed with two accelerometers of type Bruell and Kjaer. In addition, a microphone was used to record acoustic effects. The set-up was excited by means of a commercial shaker connected to the center of the LN vessel; the shaker itself was driven by a sound generator.

Two different types of measurements have been carried out:

- by using white noise;
- by sweeping a sinus at fixed frequencies.

Preliminary results for response of the system have been obtained and show the resonance of the system at 3.8 Hz. The attenuation in displacement noise is about an order of magnitude for frequencies above 10 Hz. Detailed studies will be performed with the prototype cryolink.

6 Height regulation system

Height regulation can be achieved by supplying the isolators with air in various ways.

- Tank valve: For applications involving a constant load and where small differences in height are permissible, a tank valve can be employed. After the initial inflation, the air pressure or the operating height should be checked regularly and topped up if necessary.

- Pressure regulating system: When several air isolators are linked to a common pressure regulating valve, any lost air is replenished automatically and requires no maintenance. This system makes it possible to level systems with unknown weight distribution. The air isolators are combined into three groups and the pressure control valves are individually set in accordance with the distribution of weight (see Fig. 8). This type of air supply

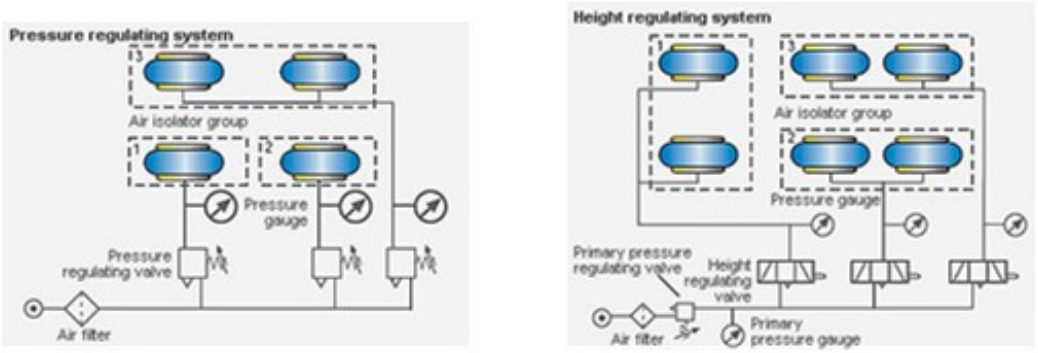

Figure 8: *Possible schemes for pressure regulating system and height regulating system.*

  can be employed only for convolution air springs and sleeve type air isolators of the type SK - so only for air isolators for which the load capacity decreases as the operating height increases.

- Height regulating system: If the height regulation has to be exceptionally accurate or if rolling lobe air springs (types SZ, RZ and LG) are used for vibration isolation, automatic height adjustment valves are required. Height regulation must always be carried out with three control valves so that the level of the machine can be adjusted via three points.

We intend to study the various schemes with the prototype. Attention will be paid to avoid wobbling motion of the LN2.

7 Studies of LN2 sloshing motion

Two-phase (liquid-gas) nitrogen flow modeling must be performed. We will focus on the study of the liquid - vapor flow inside the cryolink. The design will be optimized with respect to acoustic and mechanical noise due to bubbles. The work will be carried out in collaboration with scientists from EGO and the University of Pisa [5]. The noise spectrum is determined partly by the diameter of the bubble and the frequency of nucleation. These parameters have been studied by several researchers. In 1970 Bewilogua *et al.* [6] presented the bubble frequency as function of the diameter for several cryogenics liquid. They found for the nitrogen fluid the bubble frequency f and the bubble diameter D are correlated by the equation

$$f \cdot D^2 = 7.6 \text{ mm}^2/\text{s}. \tag{5}$$

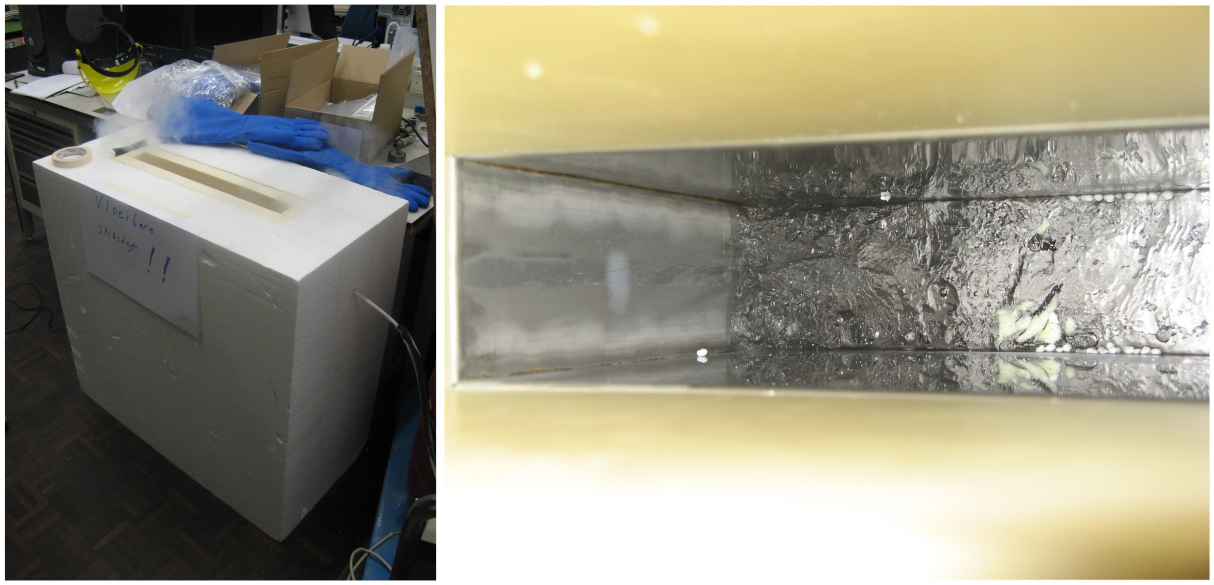

Figure 9: *Photographs of the test stand for measuring the bubbling noise in a test setup that mimics a small part of a cryolink. Noise spectra and visual information about the boiling process have been obtained.*

Fuchino *et al.* in 1996 [7] found that the correlation proposed in Eq. (5) is weakly influenced by the roughness of the surface and heating power in the case of boiling liquid nitrogen.

We have designed and constructed a test system consisting of a LN2 vessel enclosed in a 80 K environment (via isolation). The system featured a short cryolink section with actual 550 mm bath width and the full vertical length that contained a distributed heating element. Sensors were used to determine whether heat transfer takes places through convection cooling or whether bubbles are produced (microphone and visual inspection). Bubble sizes were determined and the noise spectra obtained.

8 Summary

This project note described the suspension system designed for the cryolinks for Advanced Virgo. The system must suppress the transfer of bubble noise to the beam line.

References

[1] '*On the problem of scattered light noise from AdV CryoTraps*', Irene Fiori, Virgo note in preparation (2010).

[2] Jean-Yves Vinet, Phys. Rev. **D** 56, N.10 (1997), p. 6085. Jean-Yves Vinet, Phys. Rev. **D** 56, N.10 (1997), p. 6085. Virgo note.

[3] A. Pasqualetti, https://workarea.ego-gw.it/ego2/virgo/advanced-virgo/vac/diffused-light-vs-cryotraps-11feb2010/Kcalc.pdf/ (2010).

[4] This equation is explained by Fiori as follows: the energy of the peak gets spread over a frequency band up to $f_{\max}$, thus the rms-value reduces by $1/\sqrt{f_{\max}}$. The factor $\sqrt{2}$ seems needed from simulations, although it is not completely understood. In this case, since the scattered vector completes wide (full) rotations (full rotations if $z(t) > \lambda/2$) it seems that the presence of a static phase Φ_0 can be neglected, thus the factor $1/\sqrt{2}$ that we used before, is not needed.

[5] '*Some technical notes on LN_2 boiling*', P. Di Marco, S. FilippeschiR. VIRGO-XXX (2010).

[6] '*Studies on bubble formation in low boiling liquids*', L. Bewilogua, R. Kniiner, and H. Vinzelberg, Cryogenics , February 1970.

[7] '*Influence of Surface Roughness on Transient Nucleate Boiling of Cryogens*', S. Fuchino, N. Tamada, I. Ishii, and M. Okano, Proceedings Proceedings of the Sixteenth International Cryogenic Engineering Confrence/IMCC, Kitakyushu (Japan), 1996.